Biosensors and Bioelectronics 130 (2019) 88–94

Contents lists available at ScienceDirect

Biosensors and Bioelectronics

journal homepage: www.elsevier.com/locate/bios

A amperometric immunosensor for sensitive detection of circulating tumor cells using a tyramide signal amplification-based signal enhancement system

Xiaoyan Zhou[a,1], Yujian Li[a,b,1], Haiping Wu[a], Wei Huang[b], Huangxian Ju[c], Shijia Ding[a,*]

[a] Key Laboratory of Clinical Laboratory Diagnostics (Ministry of Education), College of Laboratory Medicine, Chongqing Medical University, Chongqing 400016, China
[b] Department of Orthopaedic Surgery, The First Affiliated Hospital of Chongqing Medical University, Chongqing 400016, China
[c] State Key Laboratory of Analytical Chemistry for Life Science, School of Chemistry and Chemical Engineering, Nanjing University, Nanjing 210023, China

ARTICLE INFO

Keywords:
Electrochemical immunosensor
Circulating tumor cell
Tyramide signal amplification
Infinite coordinate polymer
HeLa cell

ABSTRACT

Herein, tyramide signal amplification (TSA)-based electrochemical immunosensor was exploited for highly sensitive detection of CTCs. In this immunosensor, the nucleolin-targeting aptamer AS1411 (CP) was used to specifically capture tumor cells, and a TSA-based signal enhancement system consisting of Pt NPs@HRP@CP composite as catalytic probe and tyramine functionalized infinite coordination polymer (ICPs@Tyr) as electroactive signal tag was applied to improve the detection sensitivity. Using HeLa cell as the model CTCs, after a sandwich reaction, CP–HeLa–Pt NPs@HRP@CP bioconjugates were formed on the electrode. Millions of ICPs@Tyr could be layer-by-layer deposited onto the target cell membrane by the catalysis of Pt NPs@HRP@CP. The developed immunorsensor could detect HeLa cell with a wide dynamic range from 2 to 2×10^4 cells/mL and a detection limit of 2 cells/mL. Most importantly, the amperometric immunosensor was successfully applied to discriminate tumor cells from white blood cells, exhibiting high specificity and sensitivity. In conclusion, this work demonstrates that the TSA-based signal enhancement system might be a potential alternative tool for the electrochemical measurement of trace amounts of CTCs in clinical diagnosis.

1. Introduction

Circulating tumor cells (CTCs), rarely shed from the original tumor or metastasis locus into peripheral blood, have been considered as an important hallmark of tumor early detection, metastasis and prognosis (De Souza et al., 2017; Thiele et al., 2017). While, accurately quantifying the exceedingly rare presence of CTCs (usually lower than 10 cells per milliliter) in the blood of cancer patients is extremely challenging. Currently, detection of CTCs is immunoaffinity-based methods, such as the Cellsearch system (Riethdorf et al., 2018), and the magnetic-activated cell sorting system (Hardingham et al., 1993), which are mainly based on immunomagnetic separation to capture and enumerate CTCs, exhibiting a high level of sensitivity and specificity. While, costly instruments and complicated operation make they are difficult to be widely implemented (Ortiz and Yu, 2018). Recently, micro-fluidic chip, depending on the different size or cell surface marker between tumor cells and normal cells, has made breakthroughs in the field of CTCs analysis (Jan et al., 2018; Shields et al., 2015). However, complex manufacturing technology of microarrays and chips is the limiting factors for further promotion (Shields et al., 2015). Thus, effective method for ultrasensitive and specific identification of these rare CTCs is urgently needed.

Nowadays, due to the simplicity and low cost, electrochemical immunosensors have attracted considerable interest in the field of laboratory and clinical analysis (Das et al., 2016; Lin et al., 2016; Povedano et al., 2018). Different electrochemical modes have been adopted for detection of tumor cells (Cao et al., 2017; Wan et al., 2014). Among them, voltammetry is popularly used due to its wide applicability and high sensitivity (Mistry et al., 2014; Piro and Reisberg, 2017; Tang et al., 2018). For example, Sun et al. fabricated an aptamer functional electrode to detect HepG2 cell based on Fe_3O_4/MnO_2/Au@Pd nanoelectrocatalysts (Sun et al., 2016). Zheng et al. developed Fe_3O_4@nanocage core-satellite hybrid nanoparticles for highly sensitive detection of MCF-7 (Zheng et al., 2014).

In voltammetry-based immunosensors, the capture of cells on the surface of the electrode can hinder the electron transfer from the electronic mediators. Thus, improving the quantity of electroactive mediators is an effective approach to enhance the current response. Infinite coordinate polymer (ICP) is a class of coordination polymerization with unique morphology and highly tailorable

* Corresponding author.
E-mail addresses: dingshijia@cqmu.edu.cn, dingshijia@163.com (S. Ding).
[1] These authors contributed equally to this work.

https://doi.org/10.1016/j.bios.2019.01.023
Received 5 November 2018; Received in revised form 31 December 2018; Accepted 17 January 2019
Available online 18 January 2019
0956-5663/

characteristics that forms from a myriad of monomer molecules incorporation (Jeon et al., 2007; Zhang et al., 2011). Recently, ferrocene formed ICPs with a uniform size and great stability can be used as electroactive mediator to efficiently transduce enzyme based biorecognition events into electronic readout (Zhang et al., 2013). In addition, the ferrocene formed ICPs exhibit an excellent redox properties and outstanding electrochemical activity compared to ferrocene monomer due to the participation of each monomer molecules in ICP (Zhang et al., 2013). Significantly, the ferrocene formed ICPs decorated with other nanomaterials can enhance not only the catalytic activity but also conductive ability, resulting in an improved electrochemical activity for target measurement (Chang et al., 2016).

Tyramide signal amplification (TSA) is widely used in immunohistochemistry for analysis of cell and nucleic acids (Akama et al., 2016; Karsten et al., 2002). In TSA technology, with the assistance of H_2O_2, horseradish peroxidase (HRP) catalyze the reporter-labeled tyramine into a short-lived reactive intermediate. These reactive intermediates can conjugate and deposit on the surrounding protein residues (including tryptophan, histidine and tyrosine residues), resulting large numbers of reporter molecules accumulation with an enhanced detection signals (as illustrated in Fig. S1, Supporting information). Based on the superior signal amplification properties, TSA has been applied in electrochemical immunosensors to improve the detection sensitivity. Tang group (Hou et al., 2014; ZHou et al., 2014) developed a series of TSA-electrochemical assays for carcinoembryonic antigen detection by in situ assembling multi-enzyme, achieving an improved analytical performance compared with the conventional sandwich-type electrochemical immunoassays. Xu et al. recently used TSA technology to deposit prussian blue-gold hybrid nanostructures on the electrode surface for detection of tissue polypeptide antigen (Xu et al., 2015). As a proven technique, TSA can increase detection sensitivity up to 100-fold compared with conventional biotin-avidin system (Van Heusden et al., 1997).

Herein, we developed a novel amperometric immunosensor for ultrasensitive detection of CTCs (HeLa cell as a model of tumor cell) via TSA induced layer-by-layer deposited electroactive ICPs. In this immunosensor, the nucleolin-targeting aptamer AS1411 (CP) is used as tumor cell catcher, and a TSA-based signal enhancement system consisting of Pt NPs@HRP@CP composite as catalytic probe and tyramine functionalized ICPs (ICPs@Tyr) as electroactive signal tag is applied to improve the detection sensitivity. Previous studies have demonstrated that nucleolin is overexpressed on the membrane of a variety of tumor cells compared with their normal counterparts (Ko et al., 2011; Wei et al., 2014; Zhang et al., 2018). Since AS1411 as nucleolin aptamer has been confirmed with excellent tumor-targeting property, it can be chosen as the capture probe to differentiate cancer cells and normal ones. In the TSA-based signal enhancement system, based on coordinate covalent bonds (Anderson et al., 2013; De Roo et al., 2016) and electrostatic attraction (Bigall et al., 2008; Chang et al., 2016), the catalytic probe is fabricated through co-immobilization of both amine-modified AS1411 (named CP for short) and HRP onto Pt NPs for capturing the HeLa cell and catalyzing the occurrence of TSA, respectively. Also, the electroactive ICPs are synthesized by infinite coordination polymerization of ferrocenedicarboxylic acid molecules under sunshine. Afterwards, ICPs@Tyr is prepared by a coupling of tyramine with ICPs. Initially, as shown in Scheme 1, the amine-modified CPs are self-assembled on a gold electrode. After 6-mercaptohexanol (MCH) blocks the nonspecific binding sites, HeLa cells are captured by the immobilized CPs. Then, the as-fabricated Pt NPs@HRP@CP nanocomposites are introduced into the immunoassay and specifically combine with the nucleolin of HeLa cytomembrane, resulting in the formation of the sandwich-like CP–HeLa–Pt NPs@HRP@CP on electrode. After that, through Pt NPs@HRP@CP catalysis reaction of H_2O_2, large number of ICPs@Tyr particles are layer-by-layer deposited on the cell surface. As a result, in the presence of HeLa cell, the combined Pt NPs@HRP catalyzes the reduction of H_2O_2 to produce abundant of O_2, thus resulting in an obvious increment of the reduction peak current of ICPs. Based on the amount of current generation, the number of cells are quantified by differential pulse voltammetry (DPV) assays. Finally, enhanced sensitivity for the detection of HeLa cells can be achieved by TSA-based layer-by-layer deposited ICPs on electrode sensing interface.

2. Material and methods

2.1. Materials

Bovine serum albumin (BSA), 1,1′-ferrocenedicarboxylic acid (FcDC), tyramine hydrochloride, chloroplatinic acid hydrate ($H_2PtCl_6{\cdot}xH_2O$), 3-(3-dimethylaminopropyl)-1-ethylcarbodiimide hydrochloride (EDC), 2-(n-morpholino) ethanesulfonic acid (MES), 6-mercapto-1-hexanol (MCH) and glutaraldehyde (GA, 25%) were purchased from Adamas (Shanghai, China). Sodium borohydride ($NaBH_4$) was purchased from Sigma-Aldrich (St. Louis, MO). Horseradish peroxidase (HRP, Rz > 3.0), hydrogen peroxide (H_2O_2, 30 wt%), citric acid, sodium citrate, 2,2'-azino-bis(3-ethylbenzothiazoline-6-sulphonic acid) (ABTS), 4',6-diamidino-2-phenylindole (DAPI) stain solution, rapid Wright-Giemsa staining solution kit and other reagents were obtained from Sangon Biotechnology Co., Ltd. (Shanghai, China). Amine functioned capture probe of the nucleolin aptamer AS1411 (5′-TTGGT GGTGGTGGTTGTGGTGGTGGTGG-3′ NH_2 C6, named CP) and 5′-fluorophore modified capture probe (for fluorescence assays, 5′FAM-TTGG TGGTGGTGGTTGTGGTGGTGGTGG-3′ NH_2 C6, named FCP) were synthesized by Sangon Biotechnology Co., Ltd. (Shanghai, China). The binding buffer contained 10 mM Tris-HCl, 10 mM KCl and 10 mM $MgCl_2$ (pH 7.4) and stored at 4 °C. Ultrapure water by Millipore Milli-Q gradient ultrapure water system (Millipore, MA) was used throughout the experiments.

2.2. Preparation of Pt NPs@HRP@CP

Briefly, 500 μL HRP (10 mg/mL), 500 μL 3′-amine modified capture probe (CP, 1 μM), and 500 μL the as-prepared Pt NPs solution (10 mg/mL) were added into 5 mL 1 × PBS containing 0.5% GA and reacted overnight under stirring at 4 °C. Finally, the solution was centrifuged and washed in 1 × PBS with 0.1% Tween-20 thrice. Then, the precipitate (designed as Pt NPs@HRP@CP) was collected and dispersed into 1 × PBS containing 0.01% Tween-20 and stored at 4 °C for the further use. For fluorescence assay, the CP was replaced by FCP to prepare Pt NPs@HRP@FCP.

2.3. Preparation of tyramine modified ICPs (ICPs@Tyr)

The bioconjugation of ICPs with tyramine was prepared through the classical carbodiimide coupling reaction. Mixed 250 μL EDC (2.5 mg/mL in ultrapure water) and 750 μL ICPs (10 mg/mL in 30 mM MES, pH 5.5) together and stirred for 10 min at room temperature. Then, 375 μL tyramine (10 mg/mL in 30 mM MES, pH 5.5) was added into the above solution and stirred for 12 h at room temperature. After that, the mixture was centrifuged and washed in 1 × PBS with 0.01% BSA to remove excess impurities. The precipitate, designed as ICPs@Tyr was dispersed into 1 × PBS containing 0.05% BSA and stored at 4 °C for the further use.

2.4. Surface modification of the gold electrode

A gold electrode (3 mm in diameter) was polished with 1.0 and 0.3 μm alumina powder to a mirror-like finish, followed by successive sonication in ultrapure water and ethanol for 5 min. Then, the electrode was activated in freshly prepared poranha solution (98% H_2SO_4: 30% H_2O_2, 3: 1 by volume) for 5 min and rinsed with ultrapure water, then dried in air. After that, 10 μL amine-modified capture probe (100 nM CP in binding buffer) was added in the cleaned gold electrode and

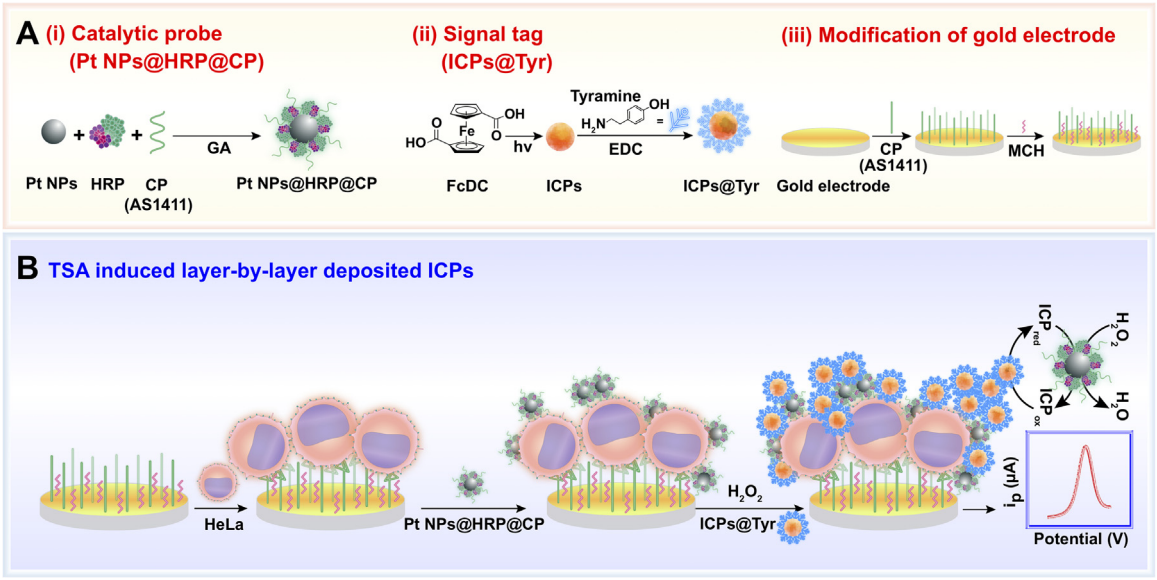

Scheme 1. The principle of electrochemical immunosensor for CTCs (HeLa cell as a model) detection based on TSA induced layer-by-layer deposited ICPs.

incubated at 37 °C for 2 h, then rinsed with ultrapure water thoroughly. To eliminate the nonspecific absorption sites at the surface of the electrode, the CP-immobilized gold electrode was incubated with 10 μL of 10 μM MCH for 1 h at room temperature, and then washed with 1 × PBS with 0.1% Tween-20. Subsequently, the modified gold electrode (MCH/CP/Gold Electrode) was further used for detection of tumor cells.

2.5. TSA-based electrochemical immunoassay

Firstly, the procedure for cell samples preparation with different numbers was supplied in Supporting information. Then, the modified gold electrode was firstly incubated with various number of HeLa (or other) cells for 60 min at 37 °C. After that, 10 μL Pt NPs@HRP@CP (2 μg/mL) was dropped on the surface of the electrode (HeLa/MCH/CP/Gold Electrode) for another 45 min at 37 °C to obtain a sandwich-like immunocomplex (Pt NPs@HRP@CP-HeLa-CP). Then, 10 μL of the prepared ICPs@Tyr (40 μg/mL) containing 0.5 mM H_2O_2 was added on the obtained sandwich-like immunosensor and reacted for 15 min at room temperature. Then, with the help of H_2O_2, tyramine was oxidized by Pt NPs@HRP to form reactive free radicals. As a result, the free radicals could covalent bind to protein residues of cell membrane and HRP. (Note: After each step, the resulting immunosensor was washed thoroughly with 1 × PBS containing 0.1% Tween-20 thrice.)

2.6. Electrochemical measurements

Electrochemical measurements were performed with a CHI 660C electrochemical analyzer (Chenhua, Shanghai, China) in a three-electrode system, including a gold electrode as working electrode, a Ag/AgCl as reference electrode and a Pt wire as auxiliary electrode. The obtained immunosensor was determined by differential pulse voltammetry (DPV) from 0.2 V to 0.8 V with a pulse amplitude of 50 mV and a pulse width of 50 ms at 50 mV/s in pH 7.0 PBS (100 mM) containing 1.5 mM H_2O_2. Cyclic voltammetry (CV) (from -0.2–0.6 V) and electrochemical impedance spectroscopy (EIS) (formal range: 10^{-2}–10^{6} Hz; potential: 220 mV; alternating voltage: 5 mV) for characterization of the fabricated immunosensor were carried out in 0.1 M KCl containing 10 mM $Fe(CN)_6^{4-/3-}$, respectively. All of the measurements were repeated three times at room temperature.

3. Results and discussion

3.1. Characterization of nanomaterials

As shown in Fig. S2A, the typical TEM images of Pt seed with a diameter of 5 nm (Bigall et al., 2008). And the Pt NPs displayed a spherical shape with an average diameter of 40 nm (Fig. S2B, C), indicating the obtained Pt NPs could provide high surface areas to immobilize amounts of HRP and capture probe (CP). Then, UV absorption spectroscopy was carried out to characterize the maximum UV absorption peak of CP (~ 260 nm), HRP (~ 280 nm and ~ 403 nm) and Pt NPs (~ 350 nm), respectively (Fig. S2D). After immobilization of HRP and amine modified CP onto Pt NPs, two new absorption peaks of Pt NPs@HRP@CP were located at ~ 260 nm and ~ 430 nm in comparison with that of the Pt NPs, indicating the successful immobilization of CP and HRP on the surface of Pt NPs. Moreover, the peroxidase catalytic activity of Pt NPs@HRP and Pt NPs was assessed by using ABTS as a substrate and the results were shown in Fig. S2E. It was clear that Pt NPs@HRP could catalyze the oxidation of ABTS in the presence of H_2O_2, resulting in an enhanced UV absorption peak compared to Pt NPs. Meanwhile, a characteristic green color (inset in Fig. S2E) was obtained in the product of Pt NPs@HRP participant, indicating the HRP decorated Pt NPs with an enhanced peroxidase catalytic activity. Thus, the catalytic probe of Pt NPs@HRP@CP was successfully prepared.

The ICPs were prepared by exposure of a methanol solution of FcDC to sunlight for 2 h, then the solution color was changed from initial yellow (inset in Fig. S3C) to taupe (inset in Fig. S3D) with the formation of ICPs. As shown in the TEM and SEM images (Fig. S3A and B), the ICPs were sphere with uniform size about 100 nm. Then, UV absorption spectroscopy was conducted for further proving the successful formation of ICPs. FcDC in methanol with distinct absorption bands related to aromatic ring (~ 220 and ~ 260 nm) and the metal-ring charge transfer (~ 318 and ~ 443 nm) (Fig. S3C) that were consistent with the previous report (Zhang et al., 2013). Compared to FcDC, the UV absorption spectra of the supernatant at ~ 318 and ~ 443 nm faded away, whereas the polymerization of ICPs displayed two obvious absorption peaks for the aromatic ring at ~ 220 and ~ 260 nm and a wide absorption peak for metal-ring charge transfer at about ~ 350 nm. These results were ascribed to the photodecomposition of FcDC leading the disappearance of metal-ring charge transfer absorption peak and the formed ICPs contained a ferrocene unit (Zhang et al., 2013). Further, tyramine was immobilized onto the ICPs, the UV absorption spectra of ICPs@Tyr

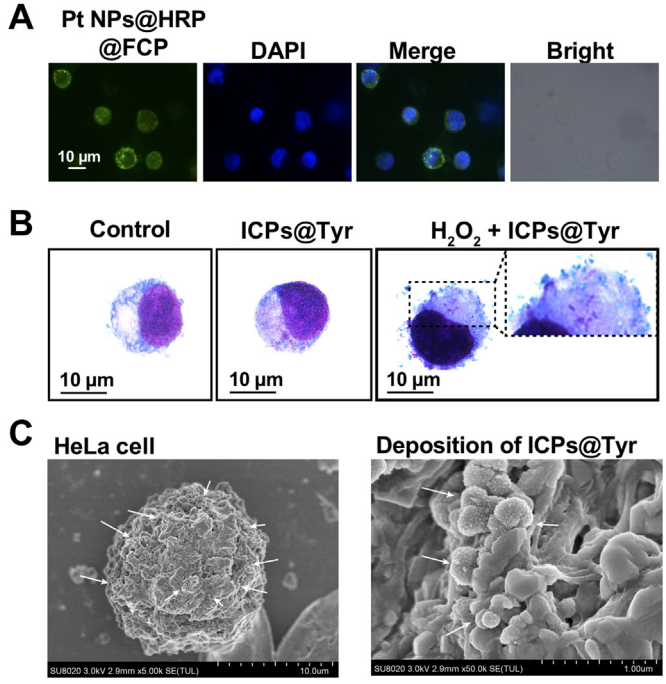

Fig. 1. (A) Fluorescence images of Pt NPs@HRP@FCP localized on HeLa cell membrane and nucleolus (green), and the nucleus (blue) were stained with DAPI. Scale bar = 10 μm. (B) Microscope photographs of HeLa cell before (left) and after ICPs@Tyr without (middle) or with (right) H_2O_2 treatment, and the enlarged cell surface (in right photograph) with large numbers of ICPs@Tyr in blue. The cells were stained by Wright-Giemsa before imaging. Scale bar = 10 μm. (C) SEM image of HeLa cell after reacted with ICPs@Tyr by Pt NPs@HRP catalysis in the presence of H_2O_2 (left, scale bar = 10 μm). The enlarged SEM image highlighted the deposition of ICPs@Tyr onto cell membrane (right, scale bar = 1.0 μm). The arrows in white indicated ICPs@Tyr.

around ~360 nm became wider owing to the cross-linking effect between ICPs and tyramine (Fig. S3D), thus proving that the signal tag of ICPs@Tyr was successfully prepared.

3.2. Characterization of ICPs deposition onto the cell membrane

We firstly measured the interaction of Pt NPs@HRP@FCP particles with HeLa cells by fluorescence microscopy. The cultured HeLa cells were detached by trypsin treatment, then Pt NPs@HRP@FCP particles were added in the resuspended cell solution to react for 30 min at 37 °C. With the help of fluorophore modified aptamer, the particles could bind to HeLa, resulting a green fluorescence signal on the cell membrane and nucleolus (Fig. 1A). After that, ICPs@Tyr with or without H_2O_2 was incubated with the above reaction product of HeLa cells for 10 min followed by staining with Wright-Giemsa. Without H_2O_2 treatment, cell image (Fig. 1B) showed no dots surrounded the cell as similar as control (untreatment HeLa cell). While, in the presence of H_2O_2, cell was covered by particles as the small blue dots, indicating ICPs@Tyr particles were successfully deposited onto the cell surface. Moreover, SEM was adopted to characterize the deposition of particles onto cell membrane. As shown in Fig. 1C, sphere structured ICPs@Tyr particles were deposited and aggregated on HeLa cell surface. These were ascribed to the covalent reaction of tyramine to tyrosine residues by the catalysis of Pt NPs@HRP, inducing large numbers of tyramine decorated ICPs depositing on the surrounding protein residues of a cell membrane.

3.3. Characterization of the fabricated immunosensor

EIS was performed in 0.1 M KCl containing 10 mM $[Fe(CN)_6]^{3-/4-}$ to characterize the process of immunosensor construction (Fig. 2A). It was observed that the bare gold electrode exhibited a small semicircle with an interface electron transfer impedance (R_{et}) value about 150 Ω, after CP and MCH modification, the resistance R_{et} increased, indicating the CP and MCH were successfully immobilized on the electrode surface in succession as excepted. The further capture of HeLa cell and Pt NPs@HRP@CP remarkably increased the electron transfer resistance, ascribed to the resistance of the interfacial electrotransfer from the cells and the proteins HRP. Significantly, after ICPs@Tyr deposited on the cell surface by Pt NPs@HRP catalysis, the R_{et} increased obviously. Due to tyramine was less conductive, the layer-by-layer deposited ICPs@Tyr on the cell surface generated an increased resistance, indicating the TSA process was completed. Besides, CV assays were applied in 0.1 M KCl containing 10 mM $[Fe(CN)_6]^{3-/4-}$ to characterize the construction and sensing process of the immunosensor. As shown in Fig. 2B, the bare gold electrode exhibited a well-defined redox peak compared to CP modified electrode. After blocking the non-specific sites with the MCH, the redox peak current apparently decreased due to the MCH hindering the electron transfer. When HeLa cells were captured on the electrode by CP, the current was further reduced for the electrical resistance of the cell. Further, the electrode incubated with Pt NPs@HRP@CP and ICPs@Tyr in the presence of H_2O_2, the redox currents gradually declined for the less conductivity of HRP and tyramine, respectively.

Moreover, the electrochemical behavious of the immunosensor for HeLa cell was detected in 100 mM PBS containing 1 mM H_2O_2. As we known, Pt NPs@HRP possessed the ability of electrocatalytic reduction of H_2O_2 to produce the amount of O_2 in detection buffer. Interestingly, the presence of O_2 could dramatically increase the reduction peak current of ICPs, resulting in effectively shuttle electrons from ICPs to the electrode surface. As shown in Fig. 2C, an extremely strong DPV signal could be detected in the presence of HeLa cell, whereas no obvious DPV signal of the immunosensor without HeLa cell. Therefore, the sandwich-type electrochemistry immunorsensor was available for HeLa

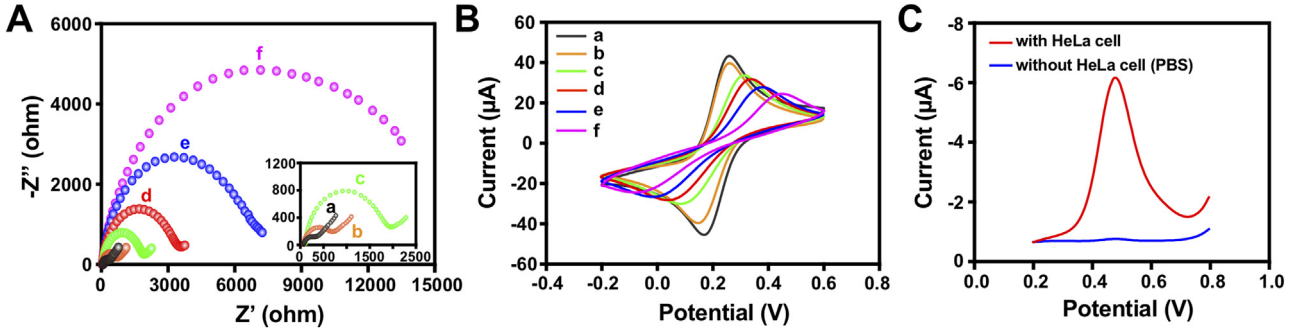

Fig. 2. (A) EIS and (B) CV of (a) bare gold electrode, (b) electrode 'a' + CP (500 nM), (c) electrode 'b' + MCH (10 μM), (d) electrode 'c' + HeLa (2×10^2 cells/mL), (e) electrode 'd' + Pt NPs@HRP@CP (2.0 μg/mL), (f) electrode 'e' + ICPs@Tyr (30 μg/mL) + H_2O_2 (0.5 mM) obtained in 0.1 M KCl containing 10 mM $[Fe(CN)_6]^{3-/4-}$. (C) DPV signal of the prepared electrochemistry immunosensor after sensing with or without HeLa cell (2×10^2 cells/mL) in 100 mM PBS containing 1.0 mM H_2O_2.

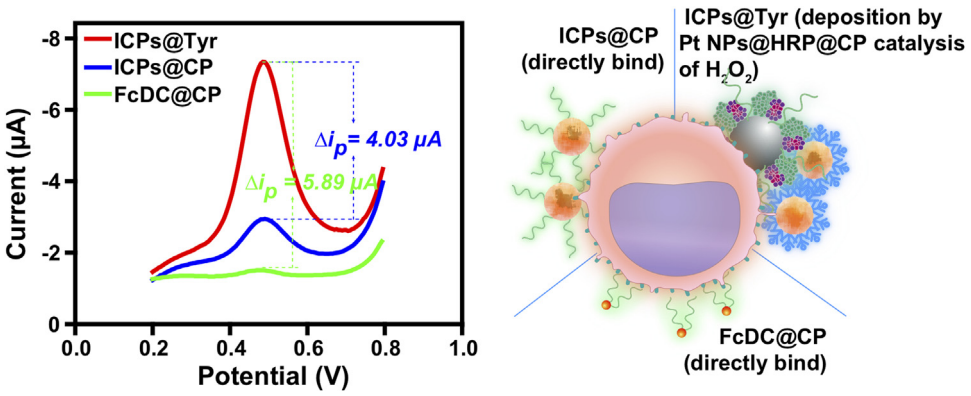

Fig. 3. Comparison of DPV signals by using ICPs@CP, FcDC@CP or ICPs@Tyr as signal tag for HeLa cell (5×10^2 cells/mL) sensing. The schematic of the manner of different signal tags in combination with HeLa cell (right).

cell detection.

3.4. Comparison of DPV responses of immunosensors based on various signal tags

To investigate the developed TSA-based immunosensor could significantly enhance electrical signal for HeLa cell detection, three types of signal tags, including ICPs@CP (immobilization of CP onto ICPs), FcDC@CP (coupling the CP to FcDC), and ICPs@Tyr were used for detection of HeLa cells (Fig. 3, the schematic diagram). After HeLa cells (5×10^2 cells/mL) were captured by the modified electrode, the preceding two signal tags of ICPs@CP and FcDC@CP were further directly combined with HeLa via CP recognition, respectively, while TSA-based ICPs@Tyr was combined with HeLa according to the procedure that mentioned above. The evaluation was made by comparison with the change in the peak currents of different signal tags in 100 mM PBS containing 1.0 mM H_2O_2. As a result, there was almost no obvious current peak after the incubation of FcDC@CP. When using TSA-based ICPs@Tyr as signal tag, a highest DPV signal was obtained compared with the other two signal tags, and shifts in the current were 4.03 μA (ICPs@Tyr versus ICPs@CP) and 5.89 μA (ICPs@Tyr versus FcDC@CP). These results were ascribed to the ultra-high electrocatalytic activity of Pt NPs@HRP composites, which could effectively increase the rate of electron transfer. Moreover, based on the powerful signal amplification ability of TSA, Pt NPs@HRP composites catalyzed the deposition of more tyramine-labeled ICPs onto the cell membrane of HeLa, resulting in superior signal enhancement compared to other signal tags based methods. Taken together, these results indicated that the application of TSA-based ICPs@Tyr in electrochemical immunosensor allowed to sensitively detect tumor cells.

3.5. Optimization of the detection conditions

Firstly, the effect of various concentrations of CP immobilization was investigated by using DPV assay of 1×10^3 cells/mL HeLa cells. With an increase in the concentration of CP, the response current increased rapidly until 100 nM CP was participated in (Fig. S4A). Then, the response current was decreased because more CP immobilized on the interface of the electrode could produce greater steric hindrance to hinder the recognition of target cells. So, the optimal concentration of CP was 100 nM. The incubation time for cells to capture affected the DPV response. As shown in Fig. S4B, the response current was significantly increased along with the prolonged incubation time until 60 min at 37 °C, then tended to plateau. Thus, 60 min was chosen as the optimal incubation time for HeLa capture. Also, concentrations of Pt NPs@HRP@CP (Fig. S4C) and ICPs@Tyr (Fig. S4D) used in the developed immunosensor were investigated. We found the response current gradually increased with increased concentration of Pt NPs@HRP@CP at 2.0 μg/mL and ICPs@Tyr at 40 μg/mL, then the response current was decreased. To HRP catalyzed oxidation of H_2O_2, tyramide radical was produced and bind to the electronrich moieties of protein (such as tyrosine residue), resulting the formation of tyramine-labeled protein (Huang et al., 2013; Watabe et al., 2011). While, the high concentration of tyramine could generate 2,2′-dihydroxydiphenyl derivatives, which could affect the response current. Therefore, 2.0 μg/mL Pt NPs@HRP@CP and 40 μg/mL ICPs@Tyr were used in the following experiments. Besides, the incubation time of the catalysis of ICPs@Tyr to deposit on the cells was investigated. As shown in Fig. S4E, at the time of 15 min, an optimal response current was obtained, indicating maximal signal tags of ICPs@Tyr had combined, which was made as the optimal ICPs@Tyr incubation time for HeLa assay. Meanwhile, the effect of H_2O_2 concentration on the electrocatalytic activity was performed by using DPV assay of HeLa (1×10^3 cells/mL) in 100 mM PBS with different H_2O_2 concentrations. The response current increased quickly with the increasing concentration of H_2O_2 at 1.5 mM, and tended to decline thereafter (Fig. S4F). Thus, 1.5 mM H_2O_2 in 100 mM PBS was adopted as the detection buffer in DPV assay.

3.6. Analytical performance

Under the optimized conditions, HeLa cell with different numbers were added into the electrochemical immunosensor to characterize the detection sensitivity of this method. As shown in Fig. 4A, DPV peak currents increased when the numbers of HeLa cell rose from 2 cells/mL to 2×10^4 cells/mL, and a linear range with logarithm of HeLa cell numbers was obtained (Fig. 4B). The linear equation was $Y = -2.527 \lg X + 0.8073$ ($R^2 = 0.9907$). Additionally, the measured detection limit toward HeLa cell was 2 cells/mL, showing a superior or comparable detection sensitivity compared with other nanomaterials-based analytical electrochemical immunosensors (Table S1). The related current to the lowest number of HeLa cells originated from ICPs which could be layer-by-layer deposited by Pt NPs@HRP nanomaterials catalyzing. Furthermore, cell membrane and HRP contained millions of tyramine binding sites, thus enriched large number of signal tags accumulation, allowing the current response to be amplified efficiently. Therefore, the developed TSA-based electrochemical immunosensor was efficient for sensitive detection of the HeLa cell.

Compared to normal cell lines, tumor cells are mostly high-expression of nucleolin on their cytomembrane (Ko et al., 2011; Wei et al., 2014; Zhang et al., 2018). Firstly, cell surface nucleolin expression levels between tumor cells (HeLa, MCF-7 and A549) and normal cells (HEK 293 and white blood cell, WBC) were assessed. As shown in Fig. S5, the HEK 293 and WBC cells showed no green fluorescence signal. While, obvious green fluorescence signals could be seen without significant difference among HeLa, MCF-7 and A549 cell lines, demonstrating nucleolin was higher expression on tumor cell cytomembrane.

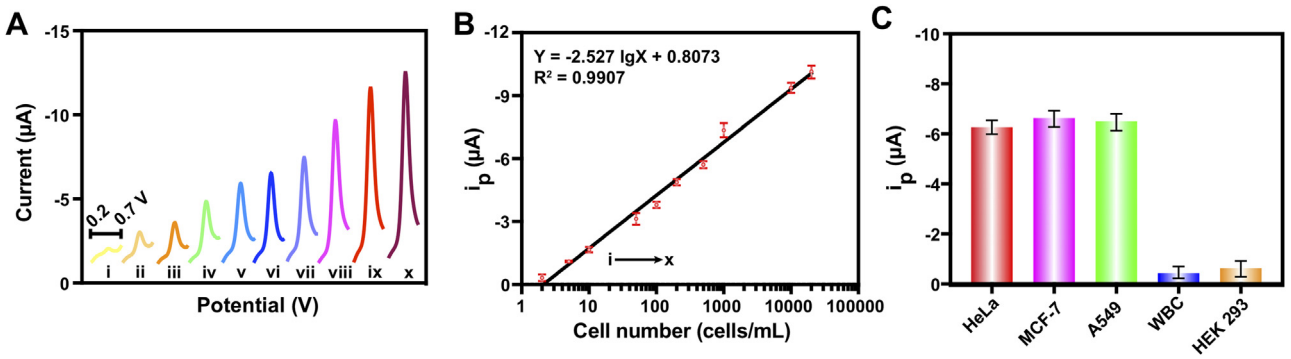

Fig. 4. (A) DPV obtained with different numbers of HeLa cell (from i to x: 2, 5, 10, 50, 1×10^2, 2×10^2, 5×10^2, 1×10^3, 1×10^4 and 2×10^4 cells/mL). (B) The plot of peak current versus the HeLa cell number. (C) Peak current in response to different cells (tumor cells: HeLa, MCF-7, A549; normal cells: WBC, HEK 293) at concentration of 1×10^3 cells/mL. Error bars were calculated from three independent experiments.

Then, these different cell lines were used to evaluate the specificity of the developed immunosensor. Under the same experimental conditions, the DPV related to different types of tumor cell (1×10^3 cells/mL) was conducted and shown in Fig. 4C. The current responses from HEK 293 and WBC were almost negligible. In contrast, high current responses were obtained from the detection of HeLa, MCF-7, and A549 cells, demonstrating the developed immunosensor with high specificity for tumor cells recognition and detection.

Moreover, the reproducibility of the immunosensor was evaluated. Briefly, five of immunosensors were adopted to assay HeLa cells (1×10^2 cells/mL) under the same experimental conditions. The current response obtained a relative standard deviation (RSD) of 3.6%, indicating a good reproducibility of the immunosensor.

3.7. Applicability of the immunosensor for HeLa cell determination

Different number of HeLa cells were added into WBC (1×10^5 cells/mL), then the mixed cell samples were analysed by the developed immunosensor. As shown in Fig. 5A, the current response was increased with the increasing number (range from 5 to 2×10^4 cells/mL) of HeLa cells that mixed with WBC. And the blank current response for 1×10^5 cells/mL WBC was 0.982 μA, which was used to calculate the Δi_p ($\Delta i_p = i_p - 0.982$). The linear relationship was obtained with a good linear equation of Y = -2.056 lgX + 0.2233 (Fig. 5B), which was comparable with that obtained from the sensitive assay. These results demonstrated that the TSA-based electrochemical immunosensor possessed great potential for detection of tumor cell with high sensitivity and accepted accuracy.

4. Conclusions

In summary, a amperometric immunosensor for the recognition and detection of circulating tumor cells was successfully constructed by using a tyramide signal amplification (TSA)-based signal enhancement system. In this system, the HRP and nucleolin-targeting aptamer bifunctionalized Pt NPs with an improved catalytic property to catalyze the deposition of tyramine-labeled electroactive signal reporters on tumor cells. There was an improvement in detection of rare tumor cells with a linear concentration range from 2 cells/mL to 2×10^4 cells/mL and a detection limit as low as 2 cells/mL. Significantly, this TSA-based immunorsensor was specific enough to discriminate tumor cells from white blood cells, attributing to the specific biorecognition between tumor cell and aptamer AS1411 on a gold electrode. Also, there is still with a challenge for us to simplify the detection procedure to meet the needs of clinical examination. Therefore, the introduction of TSA-based signal enhancement system into the electrochemical immunosensor increases the chance of detecting trace amounts of tumor cells in peripheral blood and holds great potential for precise tumor detection in clinical application.

Acknowledgements

This research was supported by the National Natural Science Foundation of China (81873980), and the Special Project for Social Livelihood and Technological Innovation of Chongqing (cstc2016shmszx130043).

Credit author statement

Xiaoyan Zhou is currently a Ph. D. of Chongqing Medical University majoring in clinical laboratory diagnosis. In the project's research, her main contribution was to design and fabricate the TSA-based immunosensor. And she is also responsible for the performance analysis of the immunosensor, data analysis and manuscript writing.

Yujian Li is currently a currently a master student of Chongqing Medical University. He is mainly responsible for cell culture and cell fluorescence related experiments. And is responsible for collecting and processing white blood cells from clinical samples.

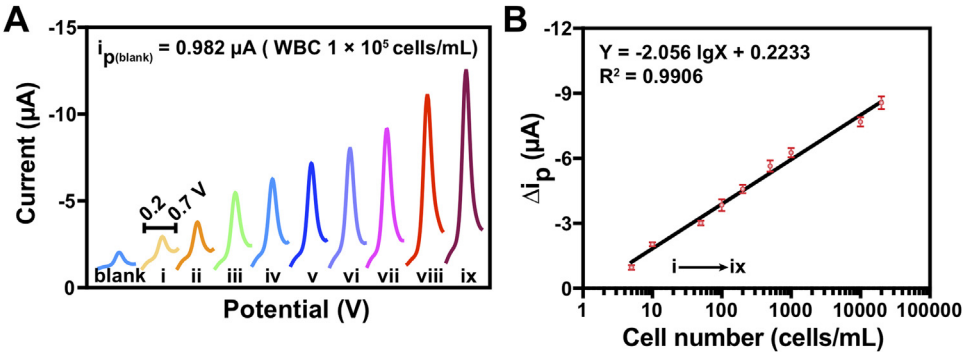

Fig. 5. (A) DPV measurement of 1×10^5 cells/mL WBC containing increasing numbers of HeLa cell (5, 10, 50, 1×10^2, 2×10^2, 5×10^2, 1×10^3, 1×10^4 and 2×10^4 cells/mL) using TSA-based electrochemical immunorsensor. (B) The relative signal in peak current (i_p) versus the number of added HeLa cells in 1×10^5 cells/mL WBC. Error bars were calculated from three independent experiments.

Haiping Wu is currently a master student of Chongqing Medical University majoring in clinical laboratory diagnosis. He is primarily responsible for the preparation and characterization of nanomaterials.

Wei Huang is currently a professor of Chongqing Medical University majoring in clinical laboratory diagnosis. He mainly conducted experiments on the sensitivity and specificity of the immunosensor.

Huang-xian Ju is a Changjiang Scholar Professor of chemistry, and Director of Key Laboratory of Analytical Chemistry for Life Science (Ministry of Education of China) in Nanjing University. He is mainly involved in guiding the design of the biosensor and the modification of the article.

Shijia Ding is currently a professor of Chongqing Medical University majoring in clinical laboratory diagnosis. As a communication author, he provided relevant financial support for the implementation of the project and participated in the principle design of the immunosensor. Check the accuracy of the relevant experimental results of this project, and finally modify and submit the article.

Declaration of interests

None.

Appendix A. Supporting information

Supplementary data associated with this article can be found in the online version at doi:10.1016/j.bios.2019.01.023

References

Akama, K., Shirai, K., Suzuki, S., 2016. Anal. Chem. 88 (14), 7123–7129.
Anderson, N.C., Hendricks, M.P., Choi, J.J., Owen, J.S., 2013. J. Am. Chem. Soc. 135 (49), 18536–18548.
Bigall, N.C., Hartling, T., Klose, M., Simon, P., Eng, L.M., Eychmuller, A., 2008. Nano Lett. 8 (12), 4588–4592.
Cao, J., Zhao, X.P., Younis, M.R., Li, Z.Q., Xia, X.H., Wang, C., 2017. Anal. Chem. 89 (20), 10957–10964.
Chang, H., Zhang, H., Lv, J., Zhang, B., Wei, W., Guo, J., 2016. Biosens. Bioelectron. 86, 156–163.
Das, J., Ivanov, I., Sargent, E.H., Kelley, S.O., 2016. J. Am. Chem. Soc. 138 (34), 11009–11016.
De Roo, J., De Keukeleere, K., Hens, Z., Van Driessche, I., 2016. Dalton Trans. 45 (34), 13277–13283.
De Souza, L.M., Robertson, B.M., Robertson, G.P., 2017. Cancer Lett. 392, 60–70.
Hardingham, J.E., Kotasek, D., Farmer, B., Butler, R.N., Mi, J.X., Sage, R.E., Dobrovic, A., 1993. Cancer Res. 53 (15), 3455–3458.
Hou, L., Tang, Y., Xu, M., Gao, Z., Tang, D., 2014. Anal. Chem. 86 (16), 8352–8358.
Huang, X., Wang, J., Liu, H., Lan, T., Ren, J., 2013. Talanta 106, 79–84.
Jan, Y.J., Chen, J.F., Zhu, Y., Lu, Y.T., Chen, S.H., Chung, H., Smalley, M., Huang, Y.W., Dong, J., Chen, L.C., Yu, H.H., Tomlinson, J.S., Hou, S., Agopian, V.G., Posadas, E.M., Tseng, H.R., 2018. Adv. Drug Deliv. Rev. 125, 78–93.
Jeon, Y.M., Heo, J., Mirkin, C.A., 2007. J. Am. Chem. Soc. 129 (24), 7480–7481.
Karsten, S.L., Van Deerlin, V.M., Sabatti, C., Gill, L.H., Geschwind, D.H., 2002. Nucleic Acids Res. 30 (2), E4.
Ko, H.Y., Choi, K.J., Lee, C.H., Kim, S., 2011. Biomaterials 32 (4), 1130–1138.
Lin, M., Song, P., Zhou, G., Zuo, X., Aldalbahi, A., Lou, X., Shi, J., Fan, C., 2016. Nat. Protoc. 11 (7), 1244–1263.
Mistry, K.K., Layek, K., Mahapatra, A., RoyChaudhuri, C., Saha, H., 2014. Analyst 139 (10), 2289–2311.
Ortiz, V., Yu, M., 2018. Trends Cell Biol.
Piro, B., Reisberg, S., 2017. Sensors 17 (4).
Povedano, E., Valverde, A., Montiel, V.R., Pedrero, M., Yanez-Sedeno, P., Barderas, R., San Segundo-Acosta, P., Pelaez-Garcia, A., Mendiola, M., Hardisson, D., Campuzano, S., Pingarron, J.M., 2018. Angew. Chem. Int. Ed. Engl. 57 (27), 8194–8198.
Riethdorf, S., O'Flaherty, L., Hille, C., Pantel, K., 2018. Adv. Drug Deliv. Rev. 125, 102–121.
Shields, C.Wt, Reyes, C.D., Lopez, G.P., 2015. Lab Chip 15 (5), 1230–1249.
Sun, D., Lu, J., Zhong, Y., Yu, Y., Wang, Y., Zhang, B., Chen, Z., 2016. Biosens. Bioelectron. 75, 301–307.
Tang, S., Shen, H., Hao, Y., Huang, Z., Tao, Y., Peng, Y., Guo, Y., Xie, G., Feng, W., 2018. Biosens. Bioelectron. 104, 72–78.
Thiele, J.A., Bethel, K., Kralickova, M., Kuhn, P., 2017. Annu. Rev. Pathol. 12, 419–447.
Van Heusden, J., de Jong, P., Ramaekers, F., Bruwiere, H., Borgers, M., Smets, G., 1997. J. Histochem. Cytochem. 45 (2), 315–319.
Wan, Y., Zhou, Y.G., Poudineh, M., Safaei, T.S., Mohamadi, R.M., Sargent, E.H., Kelley, S.O., 2014. Angew. Chem. Int. Ed. Engl. 53 (48), 13145–13149.
Watabe, S., Sakamoto, Y., Morikawa, M., Okada, R., Miura, T., Ito, E., 2011. PLoS One 6 (8), e22955.
Wei, W., He, X., Ma, N., 2014. Angew. Chem. Int. Ed. Engl. 53 (22), 5573–5577.
Xu, T., Zhang, H., Li, X., Xie, Z., Li, X., 2015. Biosens. Bioelectron. 73, 167–173.
Zhang, C., Che, Y., Zhang, Z., Yang, X., Zang, L., 2011. Chem. Commun. 47 (8), 2336–2338.
Zhang, L., Gao, X., Yang, L., Yu, P., Mao, L., 2013. ACS Appl. Mater. Interfaces 5 (16), 8120–8124.
Zhang, P., Zhao, Z., Li, C., Su, H., Wu, Y., Kwok, R.T.K., Lam, J.W.Y., Gong, P., Cai, L., Tang, B.Z., 2018. Anal. Chem. 90 (2), 1063–1067.
Zheng, T., Zhang, Q., Feng, S., Zhu, J.J., Wang, Q., Wang, H., 2014. J. Am. Chem. Soc. 136 (6), 2288–2291.
Zhou, J., Tang, J., Chen, G., Tang, D., 2014. Biosens. Bioelectron. 54, 323–328.